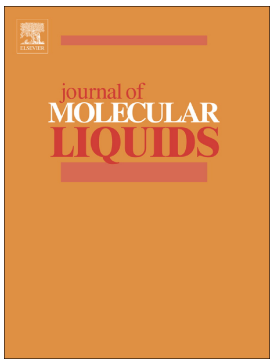

Membrane interactions of fibrillar lysozyme: Effect of lipid bilayer composition

Valeriya M. Trusova, Galyna P. Gorbenko

PII: S0167-7322(18)33779-6
DOI: https://doi.org/10.1016/j.molliq.2018.10.103
Reference: MOLLIQ 9848

To appear in: *Journal of Molecular Liquids*

Received date: 22 July 2018
Revised date: 9 September 2018
Accepted date: 20 October 2018

Please cite this article as: Valeriya M. Trusova, Galyna P. Gorbenko , Membrane interactions of fibrillar lysozyme: Effect of lipid bilayer composition. Molliq (2018), https://doi.org/10.1016/j.molliq.2018.10.103

Membrane interactions of fibrillar lysozyme: effect of lipid bilayer composition

Valeriya M. Trusova*, Galyna P. Gorbenko

Department of Nuclear and Medical Physics, V.N. Karazin Kharkiv National University, 4 Svobody Sq., Kharkiv 61022, Ukraine

*Address for correspondence:

Valeriya M. Trusova, 19-32 Geroyev Truda St., 61144 Kharkiv, Ukraine

E-mail: valerija.trusova@karazin.ua

Tel.: +38 (057) 343 82 44

Abstract

Protein polymerization into amyloid fibrils underlies a number of human disorders, including hereditary systemic amyloidosis arising from fibrillization of the mutated lysozyme. Cell membranes represent one of the main targets for the toxic action of amyloid aggregates. In the present study the impact of monomeric and fibrillar lysozyme on the structural state and physicochemical properties of the model lipid membranes composed of phosphatidylcholine and its mixtures with cardiolipin and cholesterol was investigated using the fluorescence spectroscopy technique. Probing the protein-lipid interactions with the fluorescent probes Laurdan and pyrene showed that both forms of lysozyme give rise to the dehydration of lipid bilayer and decrease of its free volume, but the magnitude of these effects was much more pronounced for the fibrillar protein. The membrane-modifying propensity of lysozyme was found to be strongly modulated by the composition of lipid bilayer, with the membrane responses being enhanced by cardiolipin and diminished by cholesterol.

1. Introduction

Protein self-association into highly ordered aggregates, amyloid fibrils, plays a pivotal role in the molecular etiology of a number of systemic and neurodegenerative human disorders including different types of amyloidosis, type II diabetes, Alzheimer's, Parkinson's and Huntington's diseases [1,2]. Amyloid fibrils represent a kind of one-dimensional pseudo-crystals of multiple characteristic length scales, characterized by translational symmetry along the fibril axis and stabilized by hydrogen bonds between the backbone amide groups and a set of hydrophobic interactions [3,4]. The self-assembly of proteins and peptides into extended linear aggregates evolves through a wide range of structural intermediates of different sizes and morphologies. Despite a well-established causative link between the formation of amyloid fibrils and evolution of severe diseases, the molecular-level details of cell damage by pathogenic protein assemblies still represents the matter of controversy. A collection of studies supports the hypothesis that cytotoxic action of amyloid aggregates is targeted primarily at cellular membranes. The major role in membrane disruption is ascribed to the early fibril intermediates, i.e. low- and higher-molecular weight oligomers whose cytotoxic potential is thought to arise from the formation of non-specific ion channels [5], the alterations in calcium homeostasis and activity of membrane enzymes [6,7] and the loss of membrane integrity [8,9]. At the same time, accumulating evidence indicates that not only the prefibrillar oligomeric species but also the mature fibrils are capable of producing the diverse membrane-modifying effects. Among these are the increase in membrane permeability [10], lipid bilayer thinning [11], membrane fragmentation [11], the uptake of lipids into the fibers growing on the membrane template [12]. An essential feature of the membrane effects of aggregated proteins is their dependence on the basic physicochemical properties of lipid bilayer, such as phase state, curvature, elasticity, electrostatic surface charge, hydrophilicity and lipid packing density, which, in turn, are controlled by the exact lipid composition. This highlights the importance of systematic studies of the model protein-lipid systems with controllable structural and physicochemical characteristics. One of such systems, containing the amyloidogenic protein lysozyme and lipid vesicles of varying composition was in the focus of our previous studies designed to shed light on the membrane-modifying action oligomeric lysozyme [13,14] and its mature fibrils [15]. Lysozyme is a multifunctional cationic protein displaying bactericidal, antitumor and immunomodulatory activities. The mutants of human lysozyme are amenable to pathological fibrillization associated with hereditary nonneuropathic systemic amyloidosis, a disease in which amyloid deposits accumulate in a range of tissues including the kidney, liver and spleen [16,17]. The ortholog of human lysozyme, hen egg white lysozyme (Lz) sharing ~60% of sequence homology, readily undergoes fibrillization in vitro and is extensively employed in the amyloid studies. Using the Lz

as a model protein we previously found that oligomeric Lz penetrates into nonpolar membrane region and increases the packing density of hydrocarbon chains [13,14], while the mature fibrils of Lz have a superficial membrane location giving rise to bilayer dehydration and more dense packing of lipid headgroups [15]. As a next logical step, in the present study the membrane interactions of the Lz mature fibrils were explored with an emphasis on the role of lipid bilayer composition. More specifically, by varying the proportion of zwitterionic (phosphatidylcholine, PC), anionic (cardiolipin, CL) phospholipids and sterol (cholesterol, Chol) in the unilamellar lipid vesicles, we addressed the following main questions: i) whether the membrane effects of fibrillar Lz depend on the surface charge of lipid bilayer; ii) how the membrane modifications induced by the Lz fibrils are modulated by cholesterol in the two- (PC/Chol) and three-component (PC/CL/Chol) lipid systems; iii) what is the location of Lz fibrils relative to the lipid-water interface. To answer these questions, several fluorescence approaches have been employed, involving the two fluorescent probes located in the polar (Laurdan) and nonpolar (pyrene) regions of a lipid bilayer, the intrinsic protein fluorescence and its quenching by a polar quencher acrylamide.

2. Materials and Methods

2.1. Materials

The hen egg white lysozyme, pyrene and cholesterol were purchased from Sigma (St. Louis, MO, USA). 1-palmitoyl-2-oleoyl-sn-glycero-3-phosphocholine and cardiolipin were from Avanti Polar Lipids (Alabaster, AL). Laurdan (6-Lauroyl-2-dimethylaminonaphthalene) was from Invitrogen Molecular Probes (Eugene, OR, USA).

2.2. Preparation of lysozyme fibrils

The lysozyme amyloid fibrils were grown by the incubation of the protein solution (10 mg/ml) in 10 mM glycine buffer (pH 2) at 60 ˚C for 14 days. The working solutions of the native and fibrillar lysozyme were prepared in 5 mM Na-phosphate buffer (pH 7.4). For the electron microscopy assay, a 10 µl drop of the protein solution was applied to a carbon-coated grid and blotted after 1 min. A 10 µl drop of 2% (w/v) uranyl acetate solution was placed on the grid, blotted after 30 sec, and then washed 3 times by deionized water and air dried. The resulting grids were viewed at Tecnai 12 BioTWIN electron microscope.

2.3. Preparation of lipid vesicles

The large unilamellar lipid vesicles were prepared by the extrusion technique from PC and its mixtures with CL (5 or 20 mol%) and/or Chol (30 mol%). The thin lipid films were obtained by the evaporation of lipids' ethanol solutions and then hydrated with 1.2 ml of 5 mM Na-phosphate buffer (pH 7.4) to yield the final lipid concentration 2 mM. Afterwards, the lipid

suspensions were extruded through a 100 nm pore size polycarbonate filter. Hereafter, the liposomes composed of binary mixtures of PC with 30 mol% Chol, 5 or 20 mol% CL were referred to as Chol30, CL5 and CL20, while the lipid vesicles composed of ternary mixtures of PC with CL (5 or 20 mol%) and Chol (30 mol%) were referred to as CL5/Chol30 and CL20/Chol30, respectively.

2.4. Fluorescence measurements

The steady-state fluorescence spectra were recorded with RF6000 spectrofluorimeter (Shimadzu, Japan). The fluorescence measurements were performed at 20 ˚C using 10 mm path-length quartz cuvettes. The excitation wavelengths were 340 nm for pyrene and 364 nm for Laurdan. The ratio of vibronic bands in the pyrene emission spectra (I_I/I_{III}) was calculated from the fluorescence intensities at 371 nm (I_I) and 382 nm (I_{III}). The excimer-to-monomer fluorescence intensity ratio (*E/M*) was determined by measuring the fluorescence intensities at the monomer (391 nm) and excimer (466 nm) peaks. The generalized polarization (GP) of Laurdan fluorescence was determined as [18]:

$$GP = \frac{I_B - I_R}{I_B + I_R} \tag{1}$$

where I_B and I_R are the fluorescence intensities of the blue (440 nm) and red (490 nm) spectral components, respectively.

The fluorescence quenching experiments were carried out with the neutral water-soluble quencher acrylamide. The emission spectra of lysozyme were recorded with excitation at 296 nm, using 5 nm band passes for both excitation and emission. Small aliquots (10 µl) of the acrylamide stock solution (4 M) were added to a stirred and temperature-controlled protein solution or protein-lipid mixtures. Fluorescence intensity measured in the presence of quencher was corrected for the reabsorption and inner filter effects using the following coefficient:

$$k = \frac{\left(1-10^{-A}\right)A_s}{\left(1-10^{-A_s}\right)A} \tag{2}$$

where A is the protein absorbance in the absence of a quencher, and A_s is the total absorbance of the sample at excitation or emission wavelengths. The fluorescence quenching data were analyzed in terms of the Stern-Volmer equation [19]:

$$I_0/I = 1 + k_q\tau_0 = 1 + K_{SV}[\mathrm{Q}] \tag{3}$$

Where I_0 and I are fluorescence intensities recorded in the absence and presence of a quencher, respectively, k_q is the bimolecular quenching rate constant, τ_0 is the fluorophore lifetime in the absence of the quencher, K_{SV} is the Stern-Volmer constant, and [Q] is the quencher concentration.

3. Results and discussion

As seen in Fig. 1, in the transmission electron microscopy images the lysozyme fibrillar aggregates are visualized as unbranched rod-like structures, up to 1.5 μm in length and 7 – 20 nm in width, lacking any trace amounts of amorphous and/or unstructured material. Under the conditions employed here, i.e. acidic pH and elevated temperature, the process of lysozyme fibrillization was reported to proceed through substantial loss of the protein tertiary structure and partial disruption of the secondary structure, resulting in the formation of assemblies with partially solvent-exposed hydrophobic patches, weakened intramolecular H-bonding, reduced hydration and high net positive charge [20].

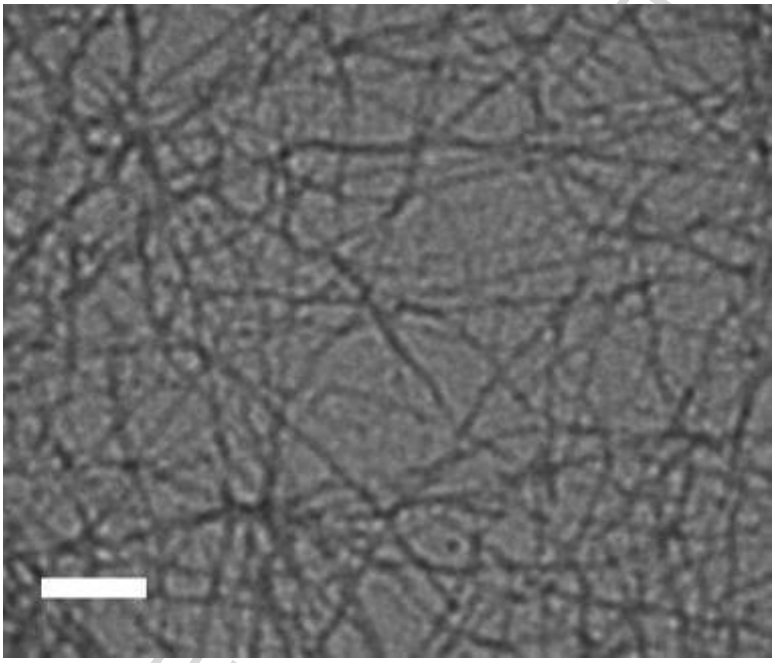

Fig. 1. Transmission electron microscopy images of lysozyme amyloid fibrils. Scale bar is 200 nm

As the first step towards elucidating the membrane effects of fibrillar lysozyme (LzF), we investigated the protein-induced modification of the polar region of lipid bilayer using the fluorescent membrane probe Laurdan which is distinguished by a high sensitivity to the degree of membrane hydration and lipid phase state [21]. This probe responds to the environmental changes by the shift of its emission maximum [22,23]. Laurdan shows a substantial bathochromic shift in fluorescence spectra with increasing solvent polarity that is attributed to the increase of the dipole moment of its naphthalene moiety upon excitation and concomitant reorientation of solvent dipoles around the excited-state dipole of the probe molecule. The sensitivity of Laurdan to solvent polarity can be illustrated by the fact that its emission maximum is ~380 nm in dodecane, ~460 nm in dimethylsulfoxide, and ~490 nm in methanol [18].

In a lipid bilayer, this amphiphilic fluorophore resides at the level of glycerol backbone, with lauric acid tail being anchored in the acyl chain region. The emission maximum of membrane-

bound Laurdan exhibits a strong dependence on the lipid phase state. In the gel phase the probe emission maximum is ~440 nm, while in the liquid crystalline phase it is ~490 nm [15]. At temperatures above the phase transition the Laurdan emission maximum shows a bathochromic shift arising from the increased hydration of the lipid bilayer at the level of glycerol backbone. In general, the Laurdan emission spectrum represents a superposition of two distinct components corresponding to the solvent-unrelaxed (shorter-wavelength band centered at ~440 nm) and solvent-relaxed states (longer-wavelength band centered at ~490 nm) [25, 26]. The variations in the degree of membrane hydration alter the ratio between these spectral components, thereby resulting in the shift of the emission maximum that is commonly quantified using the steady-state fluorescence parameter known as the generalized polarization (GP) [27].

Shown in Fig. 2 are the typical emission spectra of Laurdan measured in the absence of protein (Fig. 2A) and at varying concentrations of LzF (Fig. 2B). Analogous spectra have been recorded for all types of lipid vesicles examined here, and similar control experiments have been conducted in the presence of monomeric protein (LzN).

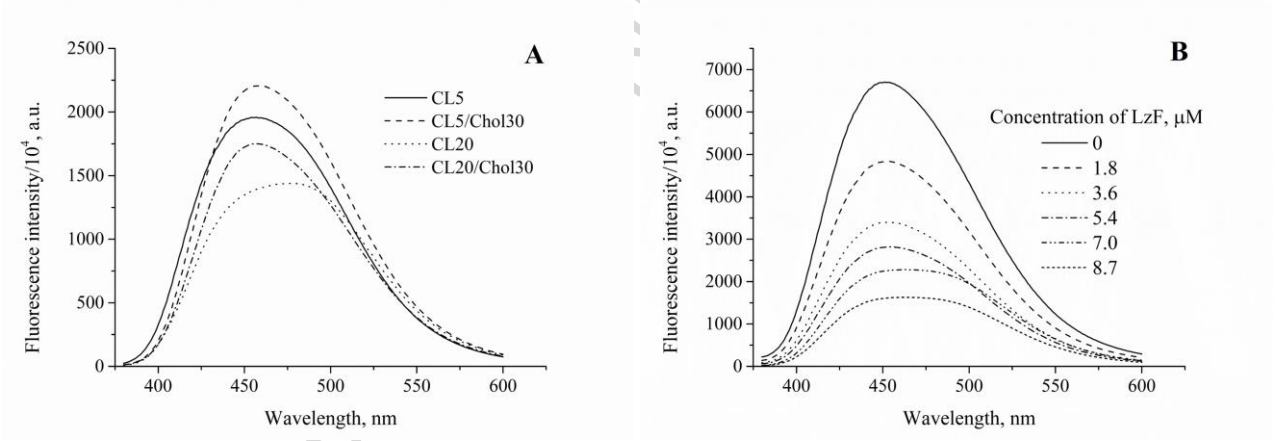

Fig. 2. Typical emission spectra of Laurdan in the model lipid membranes in the absence of protein (A). Emission spectra of Laurdan in the system CL20 + fibrillar lysozyme (B). Lipid concentration was 66 μM, Laurdan concentration was 2.3 μM

The analysis of the acquired data sets in terms of the generalized polarization showed that GP values are negative for PC liposomes and positive for all other types of liposomes, indicating that in the neat PC bilayer Laurdan resides in a more polar environment compared to the membranes from the binary and ternary lipid mixtures. The both examined forms of lysozyme, LzF and LzN brought about the increase in GP values, with the magnitude of this effect being dependent on the composition of the protein-lipid systems (Fig. 3). The rise in the Laurdan GP most likely originates from the protein-induced bilayer dehydration coupled with the increase in lipid packing density. The three main tendencies are noteworthy: i) the fibrillar lysozyme produces a more pronounced decrease in bilayer hydration compared to the monomeric protein; ii) the

modifying influence of LzF and LzN is substantially stronger in the negatively charged lipid bilayers relative to the neutral ones; iii) the membrane effects of fibrillar and, to a lesser extent, monomeric lysozyme, are considerably diminished in the presence of cholesterol.

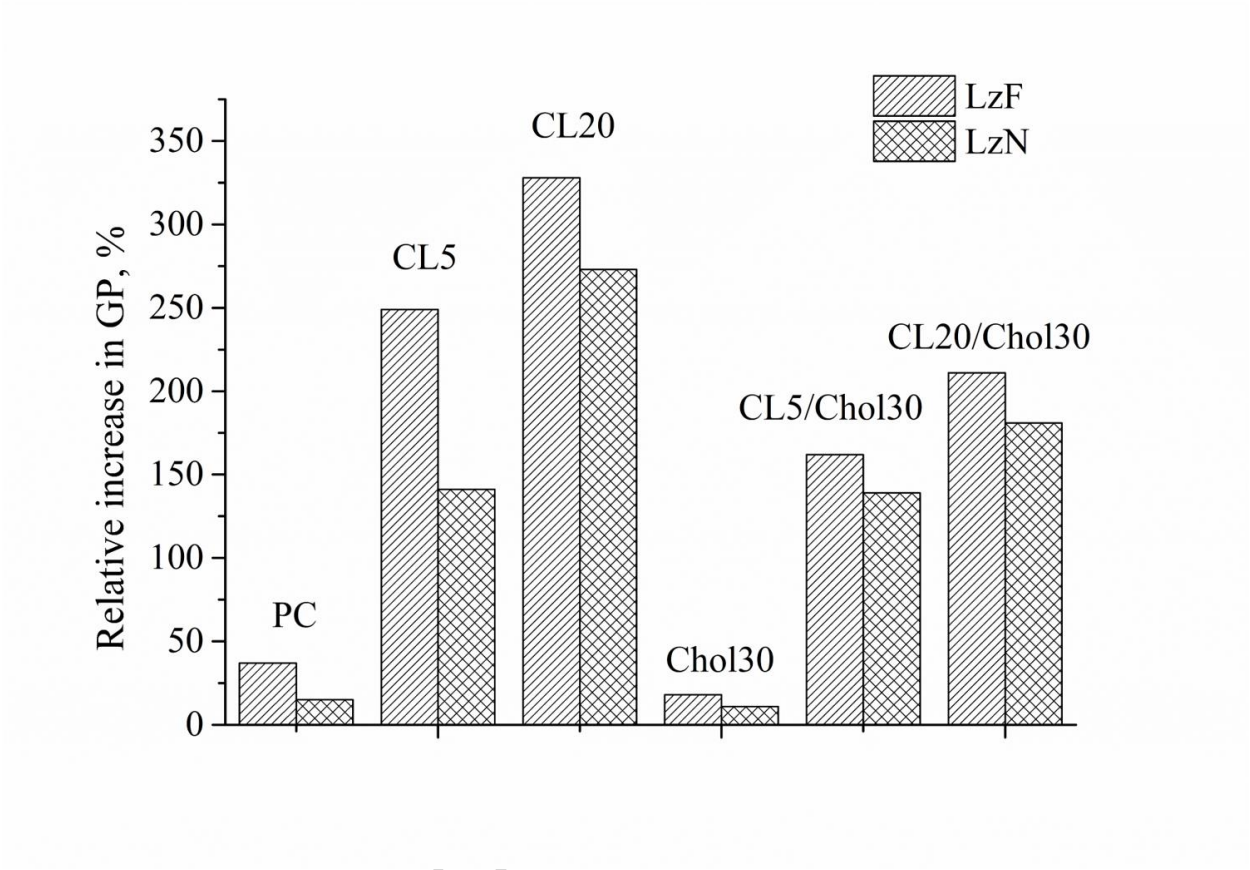

Fig. 3. Relative increase in generalized polarization of Laurdan upon binding of monomeric and fibrillar lysozyme to the lipid bilayers of various composition.

The next step of the study was directed towards uncovering the impact of the lysozyme fibrils on the structure and dynamics of nonpolar part of lipid bilayer using another fluorescent probe, pyrene, distributing in the acyl chain region. Fig. 4 depicts the representative emission spectra of pyrene in the lysozyme-lipid systems measured at varying concentrations of the aggregated protein. As can be seen, the spectra are characterized by clearly defined vibronic bands which reflect the π-π* transitions in the fluorophore molecule. Specifically, the first vibronic band (peak at 372 nm) corresponds to the 0-0 transition, while the third band (peak at 383 nm) describes the 0-2 transition [27]. Due to a strong correlation between electronic and vibronic states of pyrene molecule, the third peak proved to be extremely sensitive to the polarity of fluorophore microenvironment [28], the phenomenon manifesting itself in the increase in the intensity ratio of the first to the third vibronic band (I_I / I_{III}) in more polar solvents.

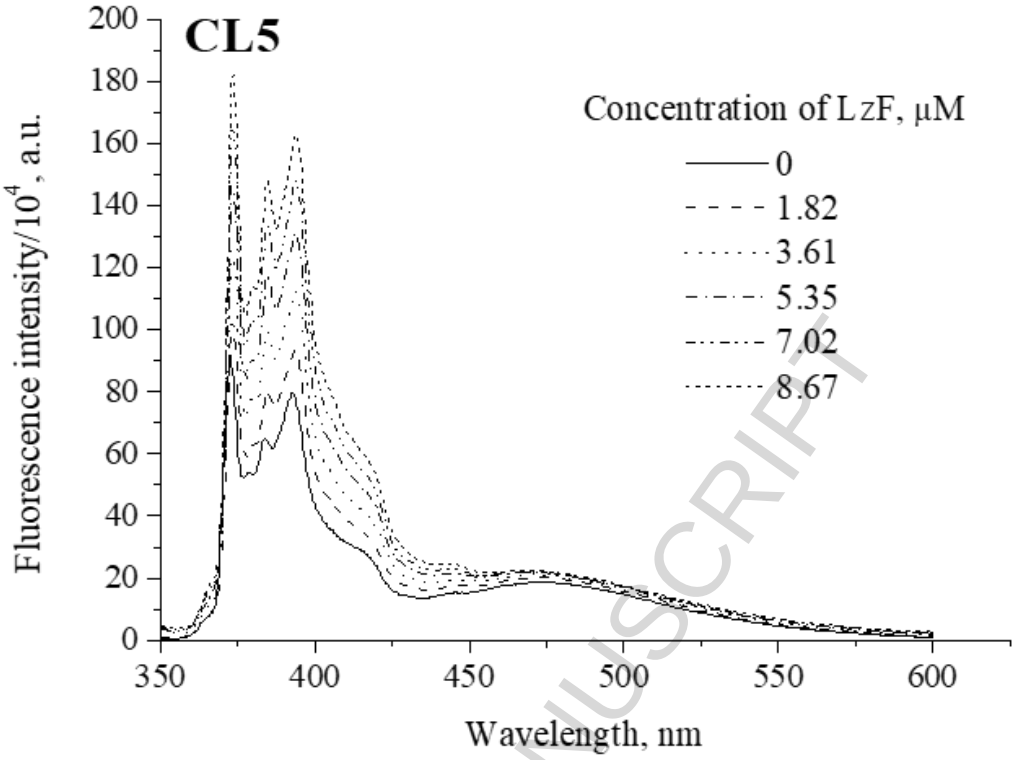

Fig. 4. Pyrene fluorescence spectra in CL5 lipid vesicles at varying concentration of fibrillar lysozyme. Lipid concentration was 66 μM, pyrene concentration was 0.8 μM

Another informative parameter that can be extracted from the pyrene fluorescence spectra is the excimer-to-monomer intensity ratio (E/M). The formation of the pyrene excimers in membrane systems is usually considered as a diffusion-controlled process, depending on the structural and dynamic properties of the lipid bilayer [27,29]. A number of models have been developed to describe the pyrene excimerization [27,28-32]. Among them, the model of "random walk" formulated by Montroll [32] and extended by Galla et al. [31] seems to be generally accepted. This model considers pyrene monomers as forming a sub-lattice on the two-dimensional periodic lattice composed of lipid molecules. The sub-lattice centers containing the excited monomers are supposed to be the traps for ground-state pyrene molecules. The average number of steps needed for ground-state molecule to reach a trapping center at a square lattice is given by:

$$\langle n_s \rangle = \frac{2}{\pi f_{Pyr}} \cdot \ln \frac{2}{f_{Pyr}} \qquad (4)$$

where f_{Pyr} is the mole fraction of the lattice centers occupied by pyrene. The relation between the collision frequency (ν_{col}) and $\langle n_s \rangle$ can be written as:

$$\nu_{col} = \langle n_s \rangle^{-1} \cdot \nu_j \tag{5}$$

here ν_j stands for the jump frequency (the number of diffusional steps per second). On the other hand, ν_{col} can be defined as:

$$\nu_{col} = \frac{E}{M \cdot \kappa} \cdot \frac{k_f}{k_f^{'}} \cdot \frac{1}{\tau_0^E} \tag{6}$$

where κ is a proportionality coefficient between the ratio of excimer-to-monomer quantum yields and fluorescence intensities, τ_0^E is the excimer lifetime, $k_f, k_f^{'}$ define the probabilities of the radiative decay of excited monomers and excimers, respectively. Eq. (6) may be simplified if one assumes that $\kappa \approx 0.8$, $k_f / k_f^{'} \approx 0.1$, $\tau_0^E \approx 38$ ns [30,31]. By combining Eqs. (4)-(6) one obtains

$$\nu_j = \frac{E}{M \cdot \kappa} \cdot \frac{k_f}{k_f^{'}} \cdot \frac{1}{\tau_0^E} \cdot \frac{2}{\pi f_{pyr}} \ln \frac{2}{f_{pyr}} \tag{7}$$

As follows from Eq. (7) there exists a direct relation between the measurable quantity E/M and the pyrene jump frequency, which, in turn, is proportional to the lateral diffusion coefficient (D_{diff}) [27,31]:

$$D_{diff} = \frac{1}{4} \cdot \nu_j \lambda^2 \tag{8}$$

here $\lambda \approx 0.8$ nm is the average jump length of the pyrene monomers. Within the framework of the above model, pyrene is considered as an indicator of the membrane free volume since the existence of free volume in the hydrophobic region of lipid bilayer controls the frequency of the collisions between the pyrene molecules and its diffusion coefficient. The membrane free volume is the result of the formation of acyl chain rotational isomers (so-called *gauche-trans-gauche* kinks) due to the thermal undulations of the lipid hydrophobic tails. The kink formation gives rise to the lateral displacement of the acyl chains creating thereby the membrane free volume. Pyrene diffusional step is thought to be completed only when the space formed upon a molecule jump, will close due to the displacement of the defect of neighboring acyl chain [29,32]. Therefore, the frequency of the pyrene diffusional steps ν_j is directly proportional to the frequency of the defect displacement along the acyl chain, ν_k:

$$\nu_j = \frac{2d_k^2}{L^2} \nu_k \tag{9}$$

where $d_k = 0.13$ nm is the lateral displacement of the acyl chain upon the kink formation, $L = 0.7$ nm is the length of the pyrene molecule.

Presented in Tables 1 and 2 are the spectral (the excimerization extent, E/M and I_I/I_{III} intensity ratio) and dynamic (ν_{col}, ν_j, ν_k and D_{diff}) characteristics of the pyrene excimerization calculated from the emission spectra using the Eqs. (4)-(9), in the absence of the protein, and in the presence of LzF or LzN. The main outcomes from the analysis of the obtained parameter set can be outlined as follows: i) both LzF and LzN exert statistically significant effect on the pyrene excimerization process only in the negatively charged CL-containing lipid vesicles (CL5, CL20, CL5/Chol30 and CL20/Chol30), where the protein-lipid complexation resulted in the decrease of all estimated parameters; ii) the influence of fibrillar species on the pyrene characteristics was markedly stronger than that of the native protein; iii) the inclusion of cholesterol into the lipid bilayer suppressed the action of LzF and LzN on the membrane properties sensed by pyrene. These findings suggest that the lysozyme, either in fibrillar or monomeric form, does not modify the free volume of the neutral vesicles, while the protein binding to the negatively charged bilayers is accompanied by the drop in the polarity of pyrene microenvironment (as judged from the decrease in I_I/I_{III}) and the reduction of the membrane free volume (as concluded from the decrease in E/M, ν_{col}, ν_j, ν_k and D_{diff}). These findings support the idea that lipid bilayer composition controls the membrane-associating properties of amyloid fibrils and governs the extent to which fibrillar proteins alter the physicochemical properties of the lipid bilayer.

Cumulatively, the Laurdan and pyrene fluorescence measurements provide a basis for the following inferences. (i) The observation that in the neutral PC and Chol30 liposomes the lysozyme fibrils does not produce any change in the pyrene parameters, but affects the Laurdan spectral behavior, suggest that LzF does interact with the uncharged membranes but its modifying effects are restricted to the interfacial bilayer region and do not propagate into the membrane core. (ii) In the CL-containing membranes strong electrostatic interactions between the negatively charged phospholipid headgroups and positively charged amino acid side chains not only promote the lysozyme membrane anchoring, but also favor the protein bilayer embedment to the level of acyl chains and occupation of the membrane free volume. All these processes slow down the pyrene diffusion and decrease the frequency of the collision between its molecules, resulting thereby in the reduced excimerization extent. Much more pronounced effects of LzF compared to LzN can be explained by the higher positive charge of the fibrillar protein and extension of the charged groups along the fibril length. Notably, the importance of electrostatic interactions in determining the mode of fibril-membrane complexation has been demonstrated for other amyloid-forming peptides and proteins [33-35].

Table 1. Pyrene spectral parameters in different protein-lipid systems

System	I_I / I_{III}			E/M		
	No protein	LzF	LzN	No protein	LzF	LzN
PC	0.95	0.94	0.95	0.39	0.37	0.38
CL5	0.96	0.72	0.89	0.44	0.28	0.33
CL20	0.96	0.64	0.71	0.52	0.39	0.45
Chol30	0.94	0.93	0.93	0.34	0.32	0.34
CL5/Chol30	0.95	0.85	0.93	0.35	0.27	0.32
CL20/Chol30	0.95	0.78	0.86	0.41	0.37	0.40

Table 2. Effect of fibrillar and monomeric lysozyme on pyrene excimerization parameters

System	ν_{col}, ns^{-1}, $\times 10^{-3}$			ν_j, ns^{-1}			ν_k, ns^{-1}			D_{diff}, $sm^2\ s^{-1}$, $\times 10^{-8}$		
	No protein	LzF	LzN	No protein	LzF	LzN	No protein	LzF	LzN	No protein	LzF	LzN
PC	2.71	2.56	2.63	0.02	0.01	0.02	0.44	0.41	0.43	2.42	2.31	2.36
CL5	3.05	1.94	2.29	0.02	0.01	0.01	0.49	0.32	0.37	2.73	1.74	2.05
CL20	3.61	2.71	3.12	0.02	0.02	0.02	0.58	0.44	0.51	3.23	2.42	2.79
Chol30	2.36	2.21	2.36	0.01	0.01	0.01	0.38	0.36	0.38	2.11	1.99	2.11
CL5/Chol30	2.42	1.87	2.21	0.01	0.01	0.01	0.39	0.31	0.36	2.17	1.68	1.99
CL20/Chol30	2.83	2.56	2.77	0.02	0.01	0.01	0.46	0.42	0.45	2.55	2.31	2.49

For instance, it has been found that electrostatic attraction between the Aβ peptide and lipid headgroups represents the main driving force regulating the penetration of the amyloid fibrils into the membrane hydrophobic core [33]. (iii) Both fluorescent reporters, Laurdan and pyrene, showed that the magnitude of the protein-induced changes in the lipid bilayer characteristics was markedly lower in the Chol-containing membranes. For illustration, in the CL5 liposomes the E/M decrease was at most 25 and 36% for LzN and LzF, respectively, while in the CL5/Chol30 vesicles this parameter reduced at most by 8 and 23%, respectively. This observation is in accordance with the findings reported earlier for other amyloidogenic proteins, *viz.* for the prokaryotic hydrogenase maturation factor [36], Aβ(1-40) peptide [37] and N-terminal fragment of apolipoprotein A-I [38]. The ability of cholesterol to preclude the membrane effects of prefibrillar and fibrillar protein aggregates is generally attributed to its bilayer-rigidifying propensity that hampers protein insertion into membrane core, prevents membrane disruption and permeabilization [15,37,39].

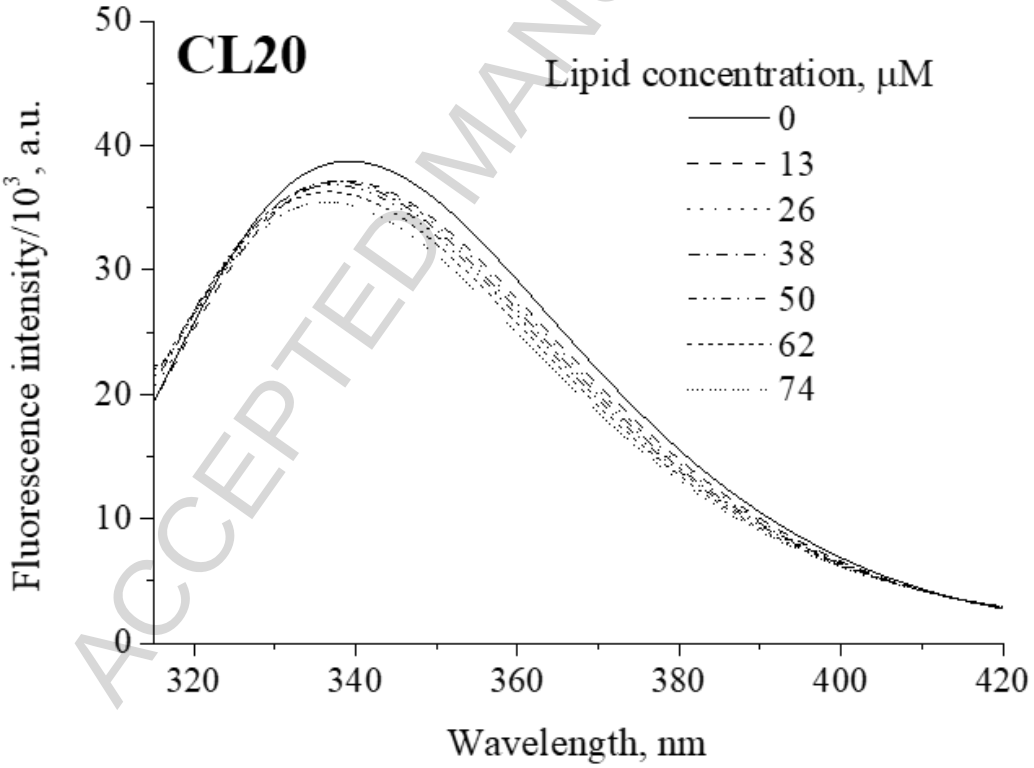

Fig. 5. Fluorescence spectra of fibrillar lysozyme in the presence of CL20 model membranes. Protein concentration was 1.6 μM.

To gain further insight into the mode of membrane association of fibrillar lysozyme, at the last step of the study we measured the protein intrinsic fluorescence and its quenching by a neutral polar quencher acrylamide. Since the major effects of the lysozyme fibrils were observed

in the CL-containing systems, in this section we restricted ourselves to the four types of lipid vesicles (CL5, CL20, CL5/Chol30 and CL20/Chol30). The hen egg white lysozyme contains six tryptophan residues located at positions 28, 62, 63, 108, 111 and 123, with Trp62 and Trp108 predominantly contributing to the overall emission spectrum of the protein [40]. The measurements of LzF intrinsic fluorescence in the presence of the negatively charged liposomes (representative spectra are depicted in Fig. 5) showed that increase of the lipid-to-protein molar ratio is accompanied by ~5 nm blue shift of the LzF emission maximum in CL5 and CL20 systems, suggesting the transfer of the protein fluorophores into the membrane environment with lower polarity. In contrast, in Chol-containing systems, as well as in the case of LzN binding to all the types of membranes, the blue shift was only ~1 nm, indicating that: i) the Trp62 and Trp108 residues of LzN adopt a more superficial bilayer location compared to LzF; and ii) cholesterol prevents the penetration of LzF into the bilayer hydrophobic core, the observation being in accordance with the pyrene fluorescence measurements.

To extract additional information, the intrinsic lysozyme fluorescence was quenched by acrylamide. As seen in Fig. 6A, acrylamide quenching is followed by the blue shift of the emission maximum for both monomeric and fibrillar forms in the presence of all types of negatively charged membranes. This finding indicates that individual Trp residues differ in their accessibility to the quencher, i.e. the solvent-exposed tryptophans are quenched more efficiently than the buried residues. This phenomenon manifests itself in the dependence of the Stern-Volmer plots on the emission wavelength (Fig. 6B).

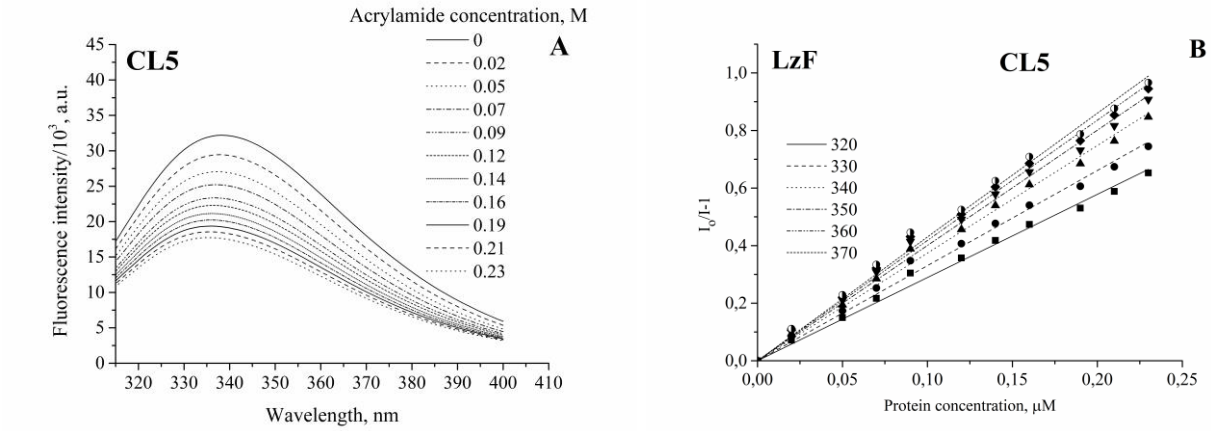

Fig. 6. Quenching of the protein intrinsic fluorescence by acrylamide in the system CL5 + fibrillar lysozyme (A). Stern-Volmer plots for the quenching of fibrillar lysozyme fluorescence by acrylamide (B). Protein concentration was 1.6 μM, lipid concentration was 74 μM.

The formation of protein-lipid complexes resulted in about two-fold decrease in Stern-Volmer constants compared to the protein in buffer solution (Table 3), suggesting the reduced accessibility of Trp residues to the solvent in the lipid-bound state. Likewise, LzF appeared to be

less exposed to acrylamide quenching than LzN assuming that stacking of the lysozyme molecules into fibrillar architecture shields the protein fluorophores from the solvent. Based on the results of molecular dynamics simulation previously we proposed the hypothetical structural model of the lysozyme amyloid fibrils. Briefly, this model implies that residues Gly54-Asn65 and Ile78-Thr89 constitute the cross-β fibril core with Trp62, one of the main protein emitters, and Trp63 locating almost in the fibril center [41]. This sterically hinders the collisions between tryptophans and acrylamide and weakens the overall quenching efficiency. Alternatively, one may suppose that close packing of monomer subunits within the protofilaments reduces the accessibility of the protein fluorophores to the quencher.

Table 3. Stern-Volmer constants for acrylamide quenching of lysozyme intrinsic fluorescence

Lipid system		Emission wavelength, nm					
		320	**330**	**340**	**350**	**360**	**370**
Buffer	LzF	4.68±0.06	5.11±0.06	5.33±0.05	5.74±0.07	5.92±0.05	6.17±0.06
	LzN	4.93±0.08	5.19±0.07	5.51±0.07	5.83±0.09	6.04±0.05	6.38±0.08
CL5	LzF	2.21±0.03	2.43±0.04	2.69±0.03	2.81±0.04	2.91±0.03	2.98±0.04
	LzN	2.89±0.04	3.31±0.05	3.73±0.05	4.01±0.06	4.17±0.06	4.31±0.07
CL5/Chol30	LzF	2.52±0.04	2.81±0.04	3.09±0.05	3.24±0.05	3.39±0.05	3.51±0.05
	LzN	2.56±0.03	2.84±0.04	3.19±0.04	3.42±0.05	3.55±0.05	3.65±0.06
CL20	LzF	1.96±0.03	2.18±0.03	2.42±0.04	2.47±0.04	2.51±0.05	2.59±0.03
	LzN	2.21±0.02	2.36±0.02	2.51±0.02	2.56±0.02	2.59±0.03	2.61±0.03
CL20/Chol30	LzF	1.17±0.01	1.29±0.01	1.38±0.01	1.43±0.02	1.47±0.02	1.49±0.02
	LzN	1.67±0.05	1.91±0.06	2.12±0.06	2.25±0.06	2.33±0.06	2.42±0.05

In summary, the following conclusions may be drawn from the results presented here: i) the lysozyme monomers and amyloid fibrils interact with the membranes via different modes; ii) the fibrillar form of lysozyme exerts more pronounced influence on the degree of hydration and free volume of the lipid bilayer; iii) the membrane binding of the lysozyme fibrils is predominantly initiated by electrostatic interactions, but the extent of fibril penetration into the membrane is further controlled by hydrophobic contacts; iv) lipid bilayer composition represents one of the major determinants of amyloid fibril effect on the structural and physicochemical characteristics of the lipid bilayer. Notably, our results are in accord with the data reported elsewhere. Direct evidence for the membrane disruption provoked by the lysozyme amyloid fibrils was provided by the different leakage assays [42-44]. Specifically, Hirano et al. showed

that the Lz amyloid aggregates induced the calcein leakage from the liposomes of different composition [42]. The observed effect was much more pronounced for the negatively charged lipid vesicles indicating that the electrostatic amyloid-membrane interactions are predominantly responsible for the membrane destruction. The arguments in favor of the membrane-destabilizing effects of fibrillar Lz come also from the study of Huang et al. [43]. It has been found that the lysozyme fibrils are capable of producing the hemolysis of human erythrocytes in the dose- and age-dependent manner. Such a disruptive effect on the cell membranes was attributed to the exposition of amyloid hydrophobic patches into the membrane interior, with electrostatic protein-lipid interactions being strongly required for fibril adsorption onto the lipid bilayer surface. At last, Gharibyan and co-workers have observed the release of lactate dehydrogenate from the plasma membranes of SH-SY5Y cells in the presence of Lz amyloid fibrils [44]. In addition, high positive net charge and hydrophobicity of the fibrillar lysozyme have been demonstrated to play a crucial role in triggering the apoptotic cascade. It has been hypothesized that the morphology of protein aggregates represents the main determinant of amyloid cytotoxicity.

In the above structural model of the lysozyme fibrils we suggested that the fragment embracing the residues Gly117-Leu129, which have labile unstructured or turn conformation within the fibril, anchors the fibril on the lipid matrix, the process which may results in the irreversible loss of bilayer integrity. The putative anchoring segment 117-129 is characterized by high hydrophobicity favoring its embedment into a lipid bilayer, but at the same time it contains several polar residues capable of forming contacts with lipid polar groups. Based on the above rationales, it can be assumed that the fragment 117-129 resides at the lipid polar/nonpolar interface while the fibril core is located on the membrane surface, as schematically illustrated in Fig. 7.

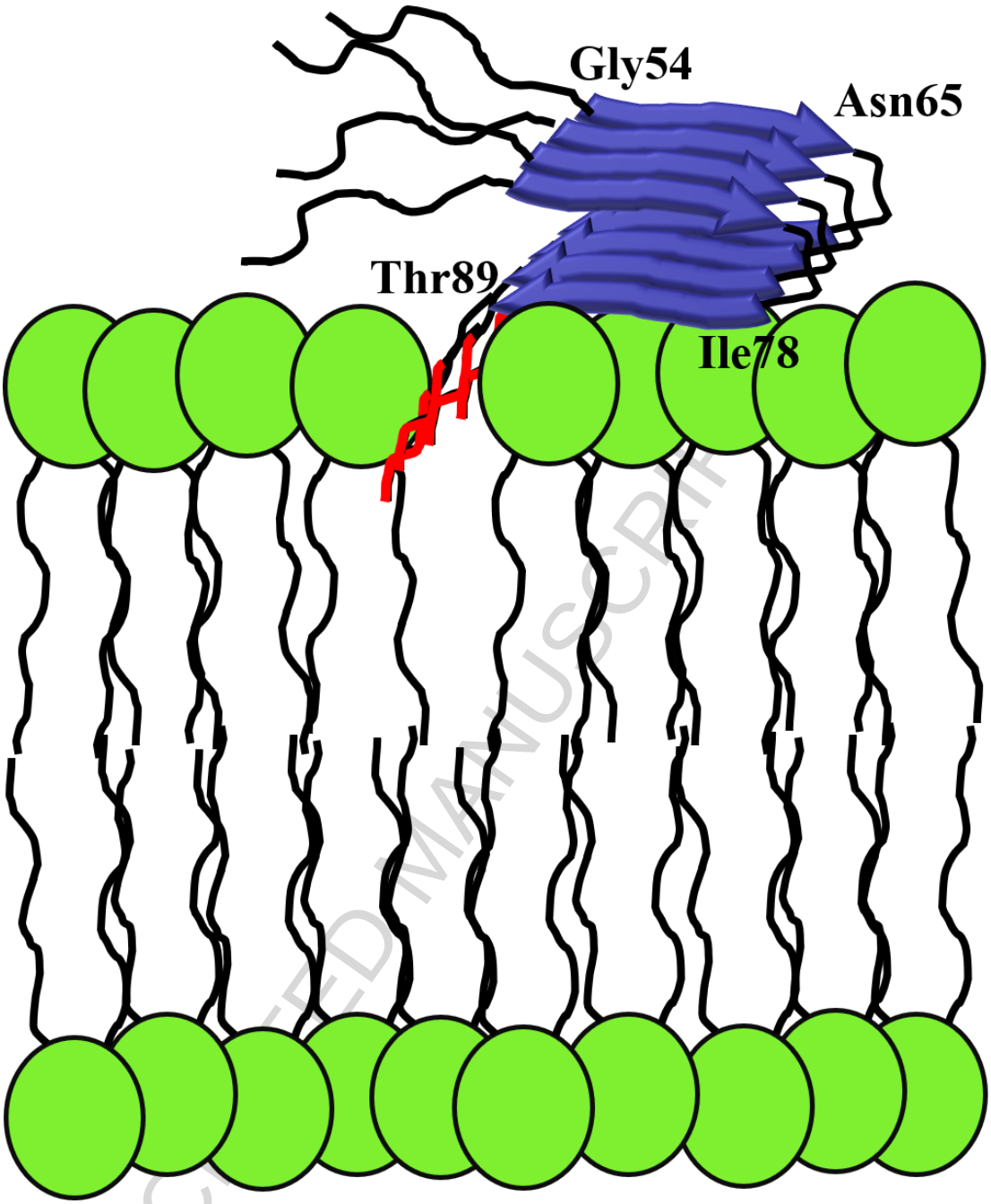

Fig. 7. Hypothetical model for orientation of lysozyme amyloid fibrils on the lipid bilayer. Shown in red is the unstructured region of the lysozyme fibrils embracing the amino acids residues Gly117-Leu129. Blue arrows indicate β-strands.

In such an orientation the lysozyme fibrils are capable of affecting both the polar and hydrophobic membrane regions as was deduced here from the Laurdan and pyrene fluorescence studies. Overall, our findings lend support to the idea that the search of effective inhibitors of fibril-membrane interactions represents the necessary step in the development of anti-amyloid strategies.

Acknowledgements

This work was partly supported by the grants No 0116U000937 and No 0117U004966 for Young Scientists from the Ministry of Education Science and of Ukraine (V.T.).

References

1. G. Wei, Z. Su, N. Reynolds, P. Arosio, I. Hamley, E. Gazit, R. Mezzenga, Self-assembling peptide and protein amyloids: from structure to tailored function in nanotechnology, Chem. Soc. Rev. 46 (2017) 4661-4708.

2. B. Meier, R. Riek, A. Böckmann, Emerging structural understanding of amyloid fibrils by solid-state NMR, Trends Biochem. Soc. 42 (2017) 777-787.

3. A. Langkilde, K. Morris, L. Seprell, D. Svergun, B. Vestergaard, The architecture of amyloid-like peptide fibrils revealed by X-ray scattering, diffraction and electron microscopy, Acta Crystallogr. D Biol. Crystallogr. 71 (2015) 882-895.

4. M. Bakou, K. Hille, M. Kracklauer, A. Spanopoulou, C. Frost, E. Malideli, L. Yan, A. Caporale, M. Zacharias, A. Kapurniotu, Key aromatic/hydrophobic amino acids controlling a cross-amyloid peptide interaction versus amyloid self-assembly, J. Biol. Chem. 292 (2017) 14587-14602.

5. B. Caughey, P. Lansbury, Protofibrils, pores, fibrils, and neurodegeneration: separating the responsible protein aggregates from the innocent bystanders, Annu. Rev. Neurosci. 26 (2003) 267-298.

6. N. Arispe, E. Rojas, H. Pollard, Alzheimer's disease amyloid beta protein forms calcium channels in bilayer membranes: blockade by tromethamine and aluminium, Proc. Natl. Acad. Sci. U.S.A. 89 (2003) 10940-10944.

7. M. Stefani, Generic cell dysfunction in neurodegenerative disorders: role of surfaces in early protein misfolding, aggregation, and aggregate cytotoxicity, Neuroscientist 13 (2007) 519-531.

8. A. Meratan, A. Ghasemi, M. Nemat-Gorgani, Membrane integrity and amyloid cytotoxicity: a model study involving mitochondria and lysozyme fibrillation products, J. Mol. Biol. 409 (2011) 826-838.

9. B. Huang, J. He, J. Ren, X. Yan, C. Zeng, Cellular membrane disruption by amyloid fibrils involved intermolecular disulfide cross-linking, Biochemistry 48 (2009) 5794-5800.

10. A. Gharibyan, V. Zamotin, K. Yanamandra, O. Moskaleva, B. Margulis, I. Kostanyan, L. Morozova-Roche, Lysozyme amyloid oligomers and fibrils induce cellular death via different apoptotic/necrotic pathways, J. Mol. Biol. 365 (2007) 1337-1349.

11. E. Sparr, M. Engel, D. Sakharov, M. Sprong, J. Jacobs, B. de Kruijf, J. Hoppener, A. Killian, Islet amyloid polypeptide-induced membrane leakage involves uptake of lipids by forming amyloid fibers, FEBS Lett. 577 (2004) 117-120.

12. M. Engel, L. Khemtemourian, C. Kleijer, H. Meeldijk, J. Jacobs, A. Verkleij, B. de Kruijff, A. Killian, J. Höppener, Membrane damage by human islet amyloid polypeptide through fibril growth at the membrane, Proc. Natl. Acad. Sci. U.S.A. 105 (2008) 6033-6038.

13. G. Gorbenko, V. Trusova, Effect of oligomeric lysozyme on structural state of model membranes, Biophys. Chem. 154 (2011) 73-81.

14. V. Trusova, G. Gorbenko, Fluorescence study on aggregated lysozyme and lipid bilayer interactions, J. Photochem. Photobiol. B: Biol. 113 (2012) 51-55.

15. A. Kastorna, V. Trusova, G. Gorbenko, P. Kinnunen, Membrane effects of lysozyme amyloid fibrils, Chem. Phys. Lipids 165 (2012) 331-337.

16. M. Pepys, P. Hawkins, D. Booth, D. Vigushin, G. Tennent, A. Souter, N. Totty, O. Nguyen, C. Blake, C. Terry, T. Feest, A. Zalin, J. Hsuan, Human lysozyme gene mutations cause hereditary systemic amyloidosis, Nature 362 (1993) 553-557.

17. M. Ahn, C. Hagan, A. Bernardo-Gancedo, E. De Genst, F. Newby, J. Christodoulou, A. Dhulesia, M. Dumoulin, C. Robinson, C. Dobson, J. Kumita, The significance of the location of mutations for the native-state dynamics of human lysozyme, Biophys. J. 111 (2016) 2358-2367.

18. T. Parasassi, E. Krasnowska, L. Bagatolli, E. Gratton, Laurdan and Prodan as polarity-sensitive fluorescent membrane probes, J. Fluoresc. 8 (1998) 365-373.

19. J. Lakowicz, Principles of Fluorescent Spectroscopy, 3d ed., 2006, Springer, New York.

20. A. Hirano, H. Yoshikawa, S. Matsushita, Y. Yamada, K. Shiraki, Adsorption and disruption of lipid bilayers by nanoscale protein aggregates, Langmuir 28 (2012) 3887-3895.

21. T. Parasassi, E. Gratton, Membrane lipid domains and dynamics as detected by Laurdan fluorescence, J. Fluoresc. 8 (1995) 365-373.

22. L. Bagatolli, E. Gratton, G. Fidelio, Water dynamics in glycosphingplipid aggregates studied by LAURDAN fluorescence, Biophys. J. 75 (1998) 331-341.

23. S. Mukherjee, A. Chattopadhyay, Monitoring the organization and dynamics of bovine hippocampal membranes utilizing Laurdan generalized polarization, Biochim. Biophys. Acta 1714 (2003) 43-55.

24. A. Lúcio, C. Vequi-Suplicy, R. Fernandez, M. Lamy, Laurdan spectrum decomposition as a tool for the analysis of surface bilayer structure and polarity: a study with DMPG, peptides and cholesterol, J. Fluoresc. 20 (2010) 473-482.

25. S. Sanchez, M. Tricerri, E. Gratton, Laurdan generalized polarization fluctuations measures membrane packing micro-heterogeneity in vivo, Proc. Natl. Acad. Sci. U.S.A. 109 (2012) 7314-7319.

26. T. Parasassi, G. De Stasio, G. Ravagnan, R. Rusch, E. Gratton, Quantitation of lipid phases in phospholipid vesicles by the generalized polarization of Laurdan fluorescence, Biophys. J. 60 (1991) 179-189.

27. Y. Barenholz, T. Cohen, E. Haas, M. Ottolenghi, Lateral organization of pyrene-labeled lipids in bilayers as determined from the deviation from equilibrium between pyrene monomers and excimers, J. Biol. Chem. 271 (1996) 3085-3090.

28. G. Bains, S. Kim, E. Sorin, V. Narayanaswami, Extent of pyrene excimer fluorescence emission is a reflector of distance and flexibility: analysis of the segment linking the LDL receptor-binding and tetramerization domains of apolipoprotein E3, Biochemistry 51 (2012) 6207-6219.

29. V. Ioffe, G. Gorbenko, Lysozyme effect on structural state of model membranes as revealed by pyrene excimerization, Biophys. Chem. 114 (2005) 199-204.

30. M.F. Blackwell, K. Gounaris, J. Barber, Evidence that pyrene excimer formation in membranes is not diffusion-controlled, Biochim. Biophys. Acta 858 (1986) 221-234.

31. H.-J. Galla, W. Hartmann, U. Theilen, E. Sackmann, On two-dimensional random walk in lipid bilayers and fluid pathways in biomembranes, J. Membr. Biol. 48 (1979) 215-236.

32. E.W. Montroll, Random walks on lattices, J. Math. Phys. 10 (1969) 753-765.

33. F. Tofoleanu, N. Buchete, Alzheimer Aβ peptide interactions with lipid membranes, Prion 6 (2012) 339-345.

34. C. Poojari, A. Kukol, B. Strodel, How the amyloid-β peptide and membranes affect each other: an extensive simulation study, Biochim. Biophys. Acta 1828 (2013) 327-339.

35. T. Choi, J. Han, C. Heo, S. Lee, H. Kim, Electrostatic and hydrophobic interactions of lipid-associated α-synuclein: the role of a water-limited interfaces in amyloid fibrillation, Biochim. Biophys. Acta, 2018, *in press*, https://doi.org/10.1016/j.bbamem.2018.02.007

36. C. Canale, S. Torrassa, P. Rispoli, A. Relini, R. Rolandi, M. Bucciantini, M. Stefani, A. Gliozzi, Natively folded HypF-N and its early amyloid aggregates interact with phospholipid monolayers and destabilize supported phospholipid bilayers, Biophys. J. 91 (2006) 4575-4588.

37. I. Sponne, A. Fifre, V. Koziel, T. Oster, J.-L. Oliver, T. Pilot, Membrane cholesterol interferes with neuronal apoptosis induced by soluble oligomers but not fibrils of amyloid-beta peptide, FASEB J. 838 (2004) 836-838.

38. V. Trusova, G. Gorbenko, M. Girych, E. Adachi, C. Mizuguchi, R. Sood, P. Kinnunen, H. Saito, Membrane effects of N-terminal fragment of apolipoprotein A-I: a fluorescent probe study, J. Fluoresc. 25 (2015) 253-261.

39. M. Sciacca, F. Lolicato, G. Di Mauro, D. Milardi, L. D'Urso, C. Satriano, A. Ramamoorthy, C. La Rosa, The role of cholesterol in driving IAPP-membrane interactions, Biophys. J. 111 (2016) 140-151.

40. G. Gorbenko, V. Ioffe, P. Kinnunen, Binding of lysozyme to phospholipid bilayers: evidence for protein aggregation upon membrane association, Biophys. J. 93 (2007) 140-153.

41. V. Trusova, G. Gorbenko, Molecular dynamics simulations of lysozyme-lipid systems: probing the early steps of protein aggregation, J. Biomol. Struct. Dyn. 36 (2017) 2249-2260.

42. A. Hirano, H. Yoshikawa, S. Matsushita, Y. Yamada, K. Shiraki, Adsorption and disruption of lipid bilayers by nanoscale protein aggregates, Langmuir 28 (2012) 3887-3895.

43. B. Huang, J. He, J. Ren, X.-Y. Yan, C.-M. Zheng, Cellular membrane disruption by amyloid fibrils involved intermolecular disulfide cross-linking, Biochemistry 48 (2009) 5794-5800.

44. A. Gharibyan, V. Zamotin, K. Yanamandra, O. Moskaleva, B. Margulis, I. Kostanyan, L. Morozova-Roche, Lysozyme amyloid oligomers and fibrils induce cellular death via different apoptotic/necrotic pathways, J. Mol. Biol. 365 (2007) 1337-1349.

Highlights:

- Lz monomers and fibrils interact with the membranes via different modes;
- Lz fibrillar form exerts more pronounced influence on lipid bilayer;
- membrane binding of the Lz fibrils is initiated by electrostatic interactions;
- lipid bilayer composition is one of the major determinants of amyloid toxicity.